Dissection of the ATPase active site of McdA reveals the sequential steps essential for carboxysome distribution

Pusparanee Hakim, Y Hoang, and Anthony G. Vecchiarelli*
Department of Molecular, Cellular, and Developmental Biology, University of Michigan, Ann Arbor, MI 48109

ABSTRACT **Carboxysomes, the most prevalent and well-studied anabolic bacterial microcompartment, play a central role in efficient carbon fixation by cyanobacteria and proteobacteria. In previous studies, we identified the two-component system called McdAB that spatially distributes carboxysomes across the bacterial nucleoid. Maintenance of carboxysome distribution protein A (McdA), a partition protein A (ParA)-like ATPase, forms a dynamic oscillating gradient on the nucleoid in response to the carboxysome-localized Maintenance of carboxysome distribution protein B (McdB). As McdB stimulates McdA ATPase activity, McdA is removed from the nucleoid in the vicinity of carboxysomes, propelling these proteinaceous cargos toward regions of highest McdA concentration via a Brownian-ratchet mechanism. How the ATPase cycle of McdA governs its in vivo dynamics and carboxysome positioning remains unresolved. Here, by strategically introducing amino acid substitutions in the ATP-binding region of McdA, we sequentially trap McdA at specific steps in its ATP cycle. We map out critical events in the ATPase cycle of McdA that allows the protein to bind ATP, dimerize, change its conformation into a DNA-binding state, interact with McdB-bound carboxysomes, hydrolyze ATP, and release from the nucleoid. We also find that McdA is a member of a previously unstudied subset of ParA family ATPases, harboring unique interactions with ATP and the nucleoid for trafficking their cognate intracellular cargos.**

Monitoring Editor
Erin Goley
Johns Hopkins University

Received: Apr 2, 2021
Revised: Aug 6, 2021
Accepted: Aug 11, 2021

INTRODUCTION

The partition protein A (ParA) family of ATPases plays major roles in the subcellular organization of bacterial cells, with members involved in the positioning of a wide array of intracellular cargos including plasmids, chromosomes, the divisome, flagella, chemotaxis clusters, and carbon-fixing organelles called carboxysomes (Lutkenhaus, 2012; Vecchiarelli *et al.*, 2012; Kiekebusch and Thanbichler, 2014). How ATP is used to organize such a diversity of genetic and proteinaceous cargos remains unclear. ParA family members are defined by the presence of a deviant Walker A motif, along with Walker A' and Walker B motifs (Koonin, 1993). Aside from these motifs that make up the ATP-binding pocket, few similarities exist at the sequence level. But structurally, all ParA family members solved to date form very similar nucleotide-sandwich dimers (Schumacher *et al.*, 2012, 2019; Zhang and Schumacher, 2017). ATP binding stabilizes dimerization because of an invariant "signature" lysine residue that defines the deviant Walker A box, which makes cross-contacts with the γ-phosphate of the opposing monomer making up the sandwich dimer (Dunham *et al.*, 2009).

The ParA family is named after its best-studied member. The ParA ATPase is part of a tripartite DNA segregation system that partitions and positions replicated copies of chromosomes and low-copy plasmids to opposite cell halves, thus ensuring faithful inheritance of these genetic cargos after cell division (Baxter and Funnell, 2014; Badrinarayanan *et al.*, 2015; Jalal and Le, 2020). Cytoplasmic ParA monomers bind ATP and form the ATP-sandwich dimer (Davey and Funnell, 1997; Zhang and Schumacher, 2017). The ParA dimer then undergoes an ATP-specific conformational change that

This article was published online ahead of print in MBoC in Press (http://www.molbiolcell.org/cgi/doi/10.1091/mbc.E21-03-0151).

*Address correspondence to: Anthony G. Vecchiarelli (ave@umich.edu).

Abbreviations used: B2H, bacterial two-hybrid; DTT, dithiothreitol; EMSA, electrophoretic mobility shift assay; McdA, Maintenance of carboxysome distribution protein A; McdB, Maintenance of carboxysome distribution protein B; mNG, monomeric NeonGreen; mTQ, monomeric Turquoise2; MU, Miller Unit; NS1, neutral site 1; nsDNA, nonspecific DNA; ParA, partition protein A; ParB, partition protein B; PCC, Pearson correlation coefficient; RbcS, Rubisco enzyme; Rubisco, ribulose-1,5-bisphosphate carboxylase/oxygenase.

licenses binding to nonspecific DNA (nsDNA) in vitro, which equates to binding the bacterial nucleoid in vivo (Hester and Lutkenhaus, 2007; Castaing *et al.*, 2008; Vecchiarelli *et al.*, 2010). In its DNA-binding form, ParA can robustly interact with its partner protein, partition protein B (ParB; Pratto *et al.*, 2008). ParB dimers site-specifically load onto the plasmid, or chromosome, to be partitioned via specific binding to a centromere-like site, typically called *parS* (Baxter and Funnell, 2014; Jalal and Le, 2020). ParB dimers spread from *parS* onto flanking DNA to form a massive multimeric nucleoprotein complex (Sanchez *et al.*, 2015; Funnell, 2016). This ParB-*parS* complex can interact with ParA dimers and stimulate its ATPase activity, which is coupled to ParA release from the nucleoid (Hwang *et al.*, 2013; Vecchiarelli *et al.*, 2013; Volante and Alonso, 2015). The resulting ParA depletion zone that forms around the ParB-*parS* complex also provides a ParA concentration gradient on the nucleoid. In this Brownian-ratchet mechanism, ParB-*parS* complexes on newly replicated chromosomes or plasmids are bidirectionally segregated to opposing cell-halves as they chase higher concentrations of ParA along the nucleoid in opposing directions (Vecchiarelli *et al.*, 2010, 2014).

A growing list of protein-based cargos have been shown to also require a ParA-type ATPase for their subcellular organization, including carboxysomes (Lutkenhaus, 2012; Vecchiarelli *et al.*, 2012). Carboxysomes are carbon-fixing organelles found in all cyanobacteria and most carbon-fixing proteobacteria (Turmo *et al.*, 2017) and are responsible for roughly a third of global carbon fixation (Cohen and Gurevitz, 2006). By encapsulating the enzymes ribulose-1,5-bisphosphate carboxylase/oxygenase (Rubisco) and carbonic anhydrase in a selectively permeable protein shell, the resulting CO_2-rich microenvironment within carboxysomes ensures that carboxylation of ribulose-1,5-bisphosphate is favored over the undesired process of photorespiration where O_2 is fixed instead of CO_2 (Kerfeld *et al.*, 2018). Despite the importance of carboxysomes to the global carbon cycle, the mechanisms underlying their subcellular organization remain unclear.

In 2010, Savage and colleagues showed that a ParA-like ATPase, now termed Maintenance of carboxysome distribution protein A (McdA), was required for the equidistant positioning of carboxysomes down the length of the rod-shaped cyanobacterium *Synechococcus elongatus* PCC 7942 (henceforth *S. elongatus*) (Savage *et al.*, 2010). More recently, we found that McdA functions with a partner protein, called Maintenance of carboxysome distribution protein B (McdB), which associates with the carboxysome cargo and is required for the dynamic oscillatory behavior of McdA in vivo (MacCready *et al.*, 2018). ATP-bound McdA has nonspecific DNA-binding activity and McdB stimulates McdA ATPase activity as well as its release from a nsDNA substrate in vitro. From these biochemical findings, we proposed that McdB-bound carboxysomes locally stimulate the release of McdA from the nucleoid, and the resulting McdA gradients are then used to drive the movement and equidistant positioning of carboxysomes across the nucleoid region of the cell; akin to DNA partitioning by ParABS systems. However, it remains to be determined how the ATP cycle of McdA governs the molecular events required for its dynamic oscillatory patterning and the positioning of McdB-bound carboxysomes across the nucleoid.

There are notable differences that set *S. elongatus* McdA apart from classical ParA family ATPases. For example, the signature lysine residue that defines the ParA family is absent in the deviant Walker A box of McdA. Also intriguing was the finding that McdA possesses a substantially higher ATPase activity compared with ParA ATPases involved in DNA partitioning (Ah-Seng *et al.*, 2009; Vecchiarelli *et al.*, 2010; MacCready *et al.*, 2018). These differences drove us to dissect the molecular events of carboxysome positioning by McdA and identify how these steps are coupled to its ATP cycle.

Despite these differences, it was recently shown that an McdA homolog shares the adenine-nucleotide sandwich dimer structure solved for several other ParA family ATPases (Schumacher *et al.*, 2019) (Figure 1A). Additionally, many of the invariant amino acids critical for ATP-dependent functions are also conserved in McdA, with the exception of the signature lysine residue in the Walker A box (Figure 1, A and B). To dissect how ATP binding and hydrolysis mediates McdA function in carboxysome positioning, we introduced strategic amino acid substitutions in the ATP-binding pocket of McdA. The mutations are synonymous with "trap" mutants made in several well-studied ParA family members involved in the positioning of plasmids (Fung *et al.*, 2001; Libante *et al.*, 2001; Barillà *et al.*, 2005; Vecchiarelli *et al.*, 2010, 2013), chromosomes (Leonard *et al.*, 2005), the divisome (Lutkenhaus and Sundaramoorthy, 2003; Kiekebusch *et al.*, 2012; Schumacher *et al.*, 2017), flagella (Ono *et al.*, 2015; Schuhmacher *et al.*, 2015), and chemotaxis clusters (Roberts *et al.*, 2012; Ringgaard *et al.*, 2014) (summary in Figure 1C, detailed in Supplemental Table S1). The data presented in this study connect key steps in the ATP cycle of McdA to the stepwise events required for distributing McdB-bound carboxysomes across the cyanobacterial nucleoid.

RESULTS

Strategy for trapping and imaging McdA at specific steps of its ATPase cycle

We performed in vivo fluorescence microscopy to determine how McdA dynamics and carboxysome organization were altered for McdA mutants predicted to be trapped at specific steps of its ATP cycle based off synonymous mutants of biochemically characterized ParAs (summary in Figure 1C, detailed in Supplemental Table S1). To visualize carboxysomes, the fluorescent protein monomeric Turquoise2 (mTQ) was fused to the C-terminus of the small subunit of the Rubisco enzyme (RbcS) yielding RbcS-mTQ. RbcS-mTQ was expressed using a second copy of its native promoter, inserted at neutral site 1 (NS1) in addition to wild-type *rbcS* at its native locus. NS1 is a well-characterized integration site on the *S. elongatus* chromosome where insertions have been shown to have no significant effects on cellular physiology (Clerico *et al.*, 2007). To simultaneously image the McdA trap mutants in our carboxysome reporter strain, the amino acid substitutions were made in the ATP-binding pocket of an McdA variant that was N-terminally fused to the fluorescent protein monomeric NeonGreen (mNG) (Shaner *et al.*, 2013). We have previously shown that mNG-McdA is fully functional for carboxysome positioning when expressed as the only copy of McdA at its native locus (MacCready *et al.*, 2018). Finally, we also performed phase-contrast imaging to monitor for changes in cell morphology, as we have recently shown that carboxysome mispositioning in *mcdA* or *mcdB* deletion strains triggers cell elongation, which we proposed is a response to carbon limitation in this obligate photoautotroph (Rillema *et al.*, 2021).

Predicted ATP binding and dimerization mutants of McdA are diffuse in the cytoplasm and carboxysomes are mispositioned

We first set out to determine the in vivo localization pattern of McdA mutants predicted to be unbound from ATP, and its impact on carboxysome positioning. We substituted the invariant catalytic lysine to an alanine (K15A) or glutamine (K15Q) in the deviant Walker A box of McdA (Figure 1B). Synonymous mutations in

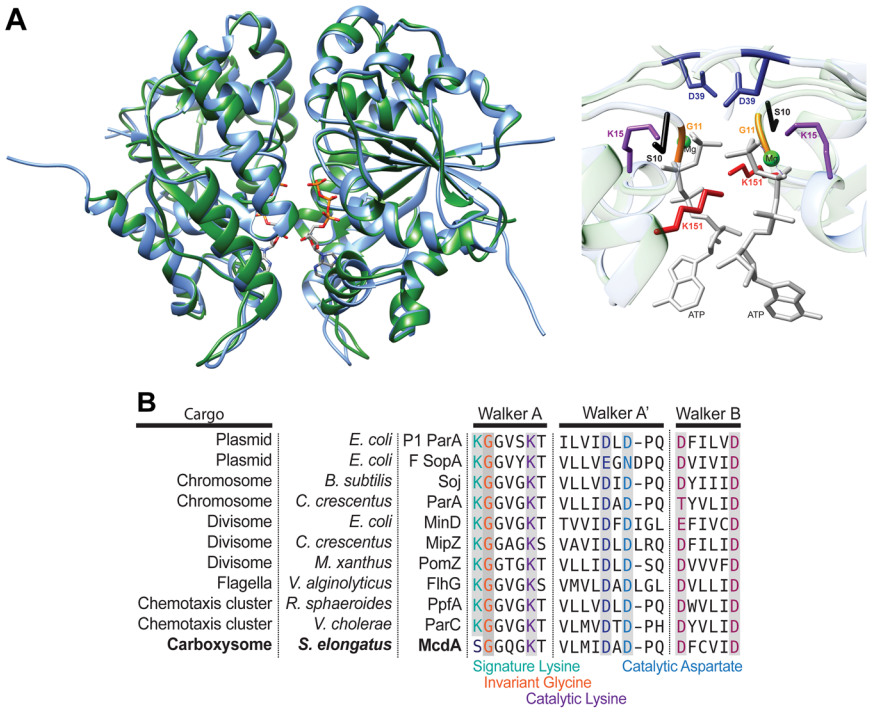

C

Residue	Mutations	ParA ATPase	Phenotype	References
Signature Lysine	K to A	MipZ MinD FlhG	ATP-binding deficient	Corrales-Guerrero *et al.* 2020 Zhou *et al.* 2005 Ono *et al.* 2015
Invariant Glycine	G to V	Soj MipZ PomZ ParC *Cc*ParA	ATP-binding proficient; Dimerization deficient	Leonard *et al.* 2005 Kiekebusch *et al.* 2012 Schumacher *et al.* 2017 Ringgaard *et al.* 2011 Ptacin *et al.* 2010; 2014
Catalytic Lysine	K to A	Soj	ATP-binding deficient	Leonard *et al.* 2005
	K to Q	MipZ PomZ ParC *Cc*ParA	ATP-binding deficient	Kiekebusch *et al.* 2012 Schumacher *et al.* 2017 Ringgaard *et al.* 2014 Ptacin *et al.* 2010; 2014
	K to R	P1 ParA *Mx*ParA	ATP-binding, dimerization and DNA-binding proficient; ATP-trapped; ATP-hydrolysis deficient	Fung *et al.* 2001; Hwang & Vecchiarelli *et al.* 2013; Vecchiarelli *et al.* 2013 Lin *et al.* 2017
Catalytic Aspartate	D to A	Soj MipZ MinD PomZ FlhG *Cc*ParA *Mx*ParA PpfA	ATP-binding, dimerization and DNA-binding proficient; ATP-trapped; ATP-hydrolysis deficient	Leonard *et al.* 2005 Thanbichler & Shapiro 2006; Kiekebusch *et al.* 2012; Corrales-Guerrero *et al.* 2020 Park *et al.* 2012 Treuner-Lange *et al.* 2013; Schumacher *et al.* 2017 Ono *et al.* 2015; Schuhmacher et al. 2015 Ptacin *et al.* 2010; 2014 Lin *et al.* 2017 Roberts *et al.* 2012

FIGURE 1: McdA shares structure and sequence conservation with ParA-type ATPases. (A) The crystal structure of *Cyanothece* McdA[D38A] (blue; PDB entry 6nop) was superimposed on to the modeled structure of *S. elongatus* McdA (green) with ATP molecules (sticks) in the sandwich dimer interface (left). The ATP-binding pocket of McdA showing amino acid residues mutated in this study (right). (B) Amino acid sequence alignment of the Walker A, A′, and B motifs conserved among ParA family ATPases. Invariant residues are shaded gray. The signature lysine (green), invariant glycine (orange) and catalytic lysine (purple) in the Walker A motif and the catalytic aspartate (blue) in the Walker A′ motif were mutated in this study. (C) Summary of strategic mutations studied in ParA family members and their associated phenotypes; Cc: *Caulobacter crescentus*, Mx: *Myxococcus xanthus*. Refer to Supplemental Table S1 for a more detailed summary of mutant phenotypes.

several other ParA-type ATPases have been shown to prevent ATP binding (Figure 1C). In wild-type *S. elongatus* cells, as shown previously, mNG-McdA oscillates on the nucleoid to equidistantly position RbcS-mTQ-labeled carboxysomes down the long axis of the cell (Figure 2A and Supplemental Movie S1). Both predicted ATP-binding mutants of McdA no longer oscillated on the nucleoid, but rather were found to be diffuse in the cytoplasm and carboxysomes were mispositioned (Figure 2, B and C, and Supplemental Movie S1). We then substituted the invariant glycine to a valine (G11V) in the deviant Walker A box of McdA (see Figure 1, B and C), which allows for ATP binding, but the bulky side-chain of valine sterically prevents dimerization (Lutkenhaus, 2012). As with the predicted ATP-binding mutants, the predicted dimerization mutant of McdA was also diffuse in the cytoplasm, and carboxysomes were no

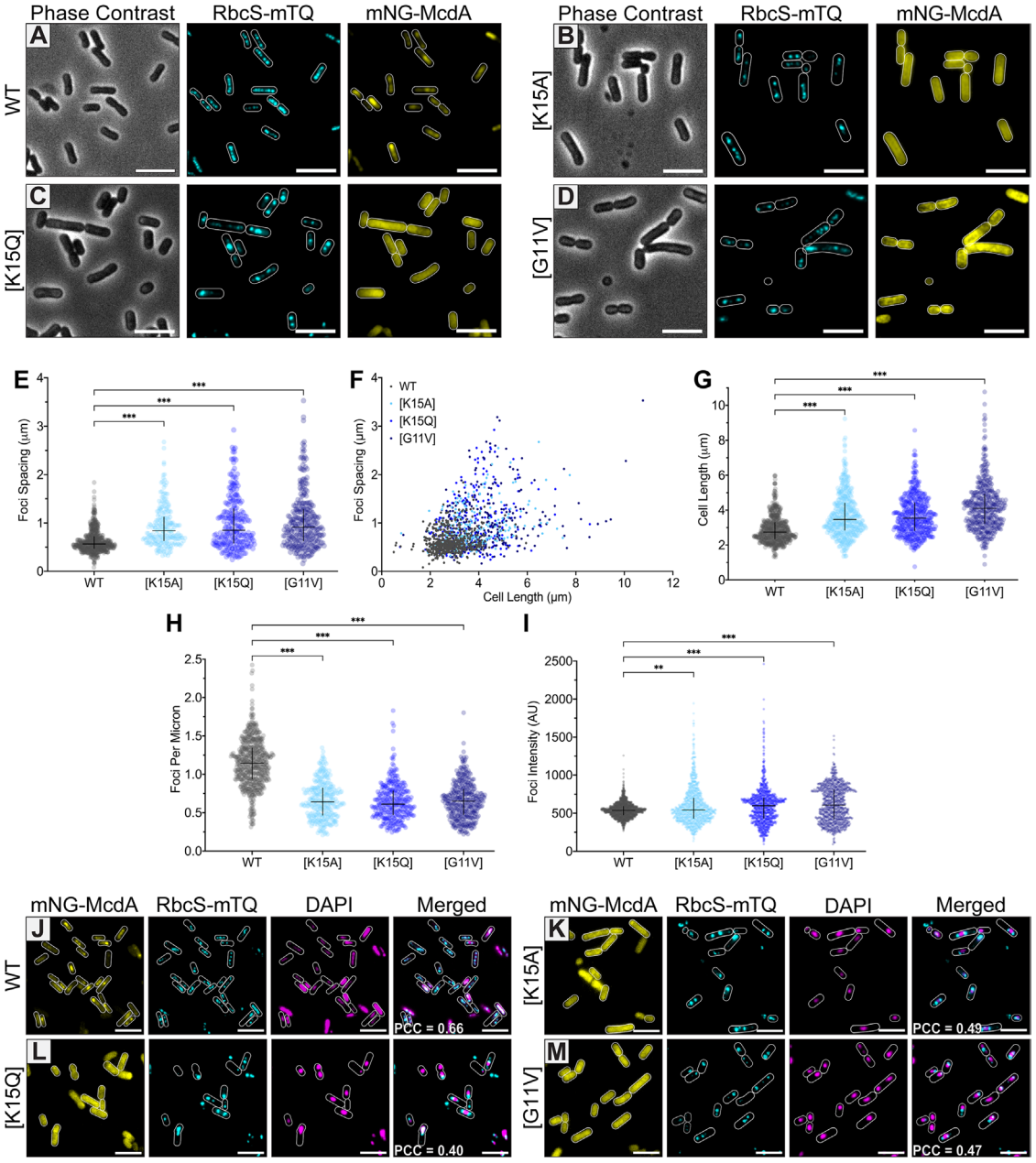

FIGURE 2: McdA mutants predicted to be deficient in ATP binding and dimerization are unable to interact with the nucleoid and position carboxysomes. (A) mNG-McdA dynamically oscillates and positions carboxysomes labeled with RbcS-mTQ (cyan). (B–D) Predicted ATP-binding (K15A and K15Q) and dimerization (G11V) mutants of mNG-McdA no longer oscillate and carboxysomes aggregate. Cell outlines in fluorescent channels are based on the phase-contrast image. (E) Spacing between carboxysome foci in the same cell. (F) Distribution of spacing between carboxysome foci as a function of cell length. For E and F: WT $n = 558$ cells; mNG-McdA[K15A] $n = 221$ cells; mNG-McdA[K15Q] $n = 236$ cells; mNG-McdA[G11V] $n = 282$ cells. (G) Cell lengths of specified strains. WT $n = 561$ cells; mNG-McdA[K15A] $n = 417$ cells; mNG-McdA[K15Q] $n = 451$ cells; mNG-McdA[G11V] $n = 408$ cells. (H) Number of carboxysome foci per unit cell length for each strain. WT $n = 578$ cells; mNG-McdA[K15A] $n = 296$ cells; mNG-McdA[K15Q] $n = 317$ cells; mNG-McdA[G11V] $n = 364$ cells. (I) Carboxysome foci intensity for each cell strain (arbitrary units = AU). WT $n = 1925$ foci; mNG-McdA[K15A] $n = 1132$ foci; mNG-McdA[K15Q] $n = 1116$ foci; mNG-McdA[G11V] $n = 1025$ foci. Data represent median with interquartile range. ***$p < 0.001$, **$p < 0.005$ by Kruskal–Wallis test. (J–M) Microscopy images of cells with ciprofloxacin-compacted nucleoids. mNG-McdA and the specified variants (yellow), carboxysome foci (cyan), and DAPI-stained nucleoids (magenta). Carboxysome and DAPI channels are merged. All PCC values were calculated from the merged RbcS-mTQ and DAPI channels from at least 300 cells per cell population. Scale bars: 5 μm.

longer uniformly distributed in the cell (Figure 2D, and Supplemental Movie S1). Immunoblot analysis against McdA showed that these mutants were expressed at levels slightly lower or similar to that of wild type (Supplemental Figure S1A). Therefore, the diffuse localization observed for these variants was not due to cleavage of the fusion proteins.

When we compared the nearest-neighbor spacing of carboxysome foci as a function of cell length, wild-type showed the same uniform spacing (0.6 ± 0.2 μm) regardless of cell length (Figure 2, E-F). All three mutants, on the other hand, displayed increased spacing, and variability in spacing, as cell length increased. The average cell lengths of the predicted ATP-binding and dimerization mutants were significantly longer compared with the wild-type strain (Figure 2G); a change in cell morphology that mirrors the Δ*mcdA* phenotype (Supplemental Figure S1B).

The increased spacing resulted in fewer carboxysome foci per unit cell length (Figure 2H). Comparing the fluorescence intensity of carboxysome foci suggested that the increased spacing in all three mutant populations was the result of carboxysome aggregation (Figure 2I). Overall, McdA mutant strains predicted to be defective for ATP binding and dimerization displayed a cell elongation phenotype, and possessed few and irregularly spaced carboxysome aggregates. These phenotypes match what we have previously observed in the *mcdA* deletion strain (Rillema *et al.*, 2021), which suggests a complete loss of function in carboxysome positioning when McdA cannot bind ATP and dimerize.

ATP binding and dimerization are predicted to be required for McdA to position carboxysomes on the nucleoid

Plasmids deleted for their ParA-type partitioning system are no longer distributed along the nucleoid. Rather, the plasmids become nucleoid "excluded" (Erdmann *et al.*, 1999; Ringgaard *et al.*, 2009; Vecchiarelli *et al.*, 2012; Planchenault *et al.*, 2020). We have shown that nucleoid exclusion also occurs for carboxysomes in *S. elongatus* strains deleted for *mcdA* (MacCready *et al.*, 2018). We set out to determine if carboxysomes are nucleoid excluded in the predicted ATP-binding and dimerization mutants of McdA. Due to the polyploid nature of *S. elongatus*, DAPI staining does not easily resolve the nucleoid region from the cytoplasm (Supplemental Figure S1C). We therefore used the gyrase inhibitor ciprofloxacin to induce nucleoid compaction (Brannudd *et al.*, 2020), which increased the cytoplasmic space observable by epifluorescence microscopy. Conveniently, when wild-type *S. elongatus* cells were treated with ciprofloxacin, mNG-McdA still oscillated on the compacted nucleoid (Supplemental Movie S2), and carboxysomes were still distributed over the nucleoid region of the cell and not in the cytoplasmic spaces. The Pearson correlation coefficient (PCC) was used to indicate the degree of colocalization (Adler and Parmryd, 2010) between the DAPI-stained nucleoid and RbcS-mTQ-labeled carboxysomes (PCC = 0.66, n = 324 cells) (Figure 2J; Supplemental Table S2). The predicted ATP-binding and dimerization mutants of mNG-McdA, on the other hand, remained diffuse in the cytoplasm and carboxysomes were nucleoid excluded, but in a surprising manner (Figure 2, K–M). Rather than having carboxysomes randomly distributed in the cytoplasmic region of the cell, the carboxysome aggregates butted up against the ends of the compacted nucleoid (Supplemental Figure S1D). As a result, the PCC values calculated for carboxysomes and the nucleoid signal were significantly lower for all three mutant strains (PCC mNG-McdA[K15A] = 0.49, n = 338 cells; mNG-McdA[K15Q] = 0.40, n = 305 cells; mNG-McdA[G11V] = 0.47, n = 365 cells) compared with the wild-type strain (PCC = 0.66, n = 324 cells). (Figure 2, J–M, merged panels, and Supplemental Table S2). A similar observation was recently found for plasmids lacking their partition system (Planchenault *et al.*, 2020), suggesting this is a widespread mesoscale phenomenon for both genetic and proteinaceous complexes in a bacterial cell.

We are currently unable to purify the McdA variants used in this study due to solubility issues. The McdA mutations made here were modeled after the biochemically characterized mutants of other ParA family proteins (summary in Figure 1C, detailed in Supplemental Table S1). Many of these ParA family ATPases have been shown to be monomeric in their apo forms and dimerize on ATP binding, which then licenses nsDNA binding in vitro or nucleoid binding in vivo (Lutkenhaus, 2012; Kiekebusch and Thanbichler, 2014). Taken together, our data suggest that ATP binding and dimerization are prerequisite steps needed for McdA to bind the nucleoid and distribute carboxysomes within the nucleoid region of the cell.

The predicted ATP-Trap mutant McdA[D39A] does not associate with the nucleoid or McdB in vivo

To solve the sandwich-dimer structure of an McdA homolog from the cyanobacterium *Cyanothece* sp. PCC 7424, the Schumacher group made an ATP-trap mutant by substituting the catalytic aspartate residue to an alanine in the Walker A' box (see Figure 1, A and B) (Schumacher *et al.*, 2019). Synonymous ParA family mutants have been shown to form ATP-bound dimers competent for DNA-binding and interaction with their cognate ParB, but are deficient in ATP hydrolysis (see Figure 1C). We made the corresponding mutation in McdA (D39A) to determine the in vivo localization pattern of an McdA mutant, presumably trapped as an ATP-bound dimer, and its effect on carboxysome positioning. Unexpectedly, mNG-McdA[D39A] was diffuse in the cytoplasm and carboxysomes were mispositioned in a manner that was identical to our predicted ATP-binding and dimerization mutants of McdA (Supplemental Figure S2A). Immunoblot analysis verified that the diffuse localization was not due to cleavage of the fusion protein (Supplemental Figure S1A). The data suggest McdA[D39A] cannot bind the nucleoid due to a loss in nonspecific DNA-binding activity. The Schumacher group showed that ATP-bound McdA[D38A] from *Cyanothece* can dimerize and bind a nsDNA substrate in vitro (Schumacher *et al.*, 2019); however, the affinities for dimerization and interaction with DNA were not compared with wild-type McdA. Since *S. elongatus* McdA is highly insoluble, we purified the McdA homolog from *Cyanothece* (*Ct*McdA) and its ATP-trap variant *Ct*McdA[D38A] (used to solve the McdA structure) and found via electrophoretic mobility shift assays (EMSAs) that *Ct*McdA[D38A] has significantly reduced DNA-binding activity compared with wild type (Supplemental Figure S2B). This finding is consistent with our in vivo observations of the corresponding mutant in *S. elongatus* (Supplemental Figure S2A). We propose McdA[D39A] is either impaired in its dimerization activity or does not go through the conformational change that licenses nucleoid binding, which our data suggest are prerequisites for McdB interaction and distributing carboxysomes over the nucleoid.

The predicted ATP-Trap mutant McdA[K15R] locks onto McdB-bound carboxysomes

We set out to construct another ATP-trap mutant of McdA that can adopt the nucleoid-binding state and interact with McdB. One of the best-studied ATP-trap mutants from the ParA family of ATPases comes from the P1 plasmid partitioning system (Fung *et al.*, 2001). Mutating the catalytic lysine to an arginine in the deviant Walker A box of P1 ParA (K122R) has shown robust in vitro and in vivo phenotypes (see Figure 1, B and C). In vitro, ParA[K122R] can bind ATP, dimerize, and bind nsDNA with an affinity comparable to wild type, but irreversibly associates with ParB because ParB cannot stimulate the ATPase activity required for releasing this association (Fung *et al.*, 2001; Vecchiarelli *et al.*, 2013). In vivo, ParA[K122R] results in a worse-than-null and dominant-negative phenotype called Par^{PD} for "propagation-defective," whereby plasmids are less stable than

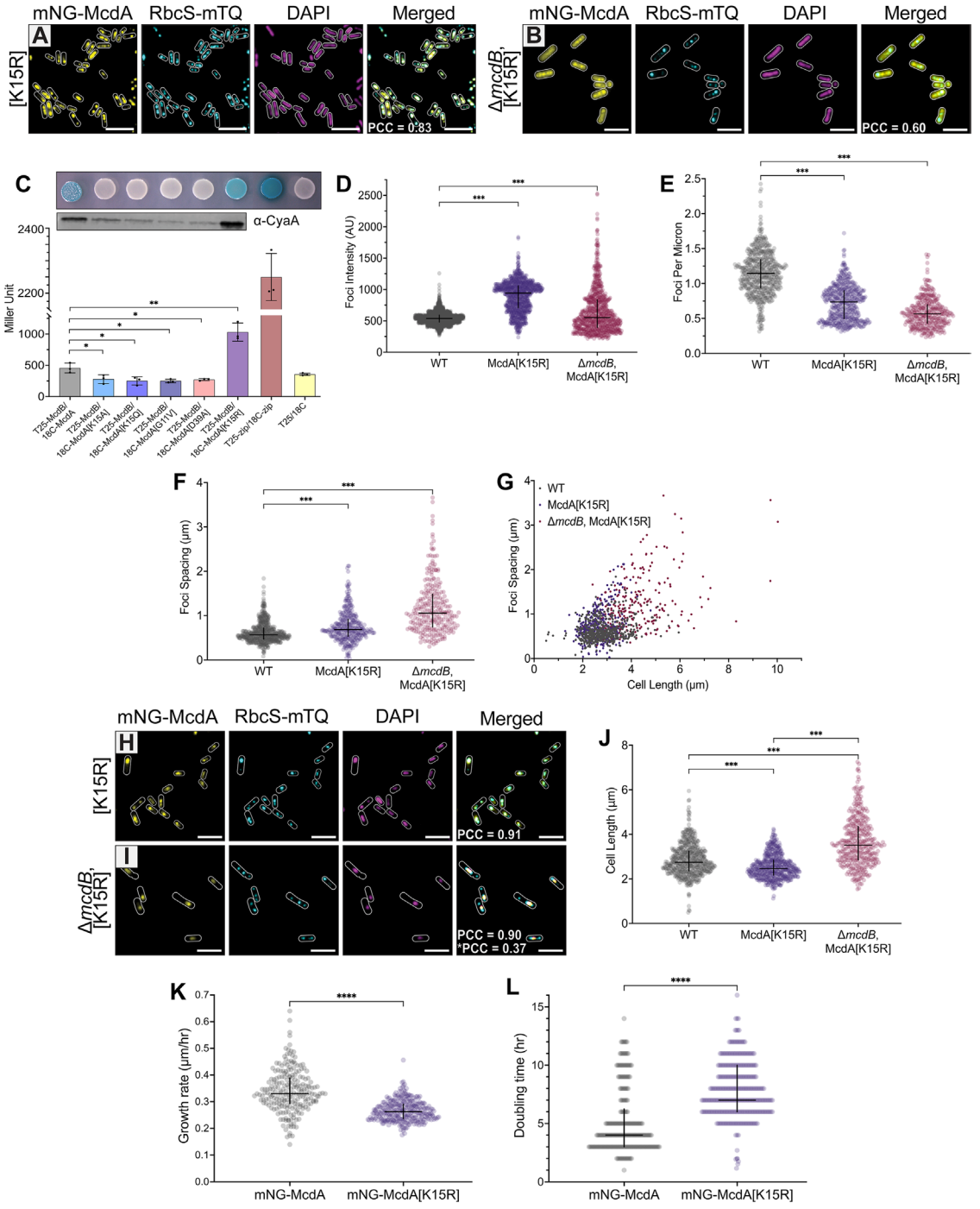

FIGURE 3: The predicted ATP-trap mutant McdA[K15R] locks McdB-bound carboxysomes onto the nucleoid. (A) Microscopy images of mNG-McdA[K15R] (yellow), RbcS-mTQ-labeled carboxysomes (cyan), and DAPI-stained nucleoid (magenta). Merged image overlays mNG-McdA[K15R] and RbcS-mTQ labeled carboxysomes with a PCC value calculated from these two signals. (B) Microscopy images of mNG-McdA[K15R] in a Δ*mcdB* background strain. Merged image shows mNG-McdA[K15R] and RbcS-mTQ-labeled carboxysomes with a PCC value calculated from these two signals. (C) (Top) B2H interaction assay between the indicated protein pairs. The image is representative of three independent experiments. (Middle) Western blot detection of T18 domain in 18C-McdA and its mutant fusions using CyaA antibody. (Bottom) Quantitative analysis of the B2H interactions. Data represent the mean and SD from three independent biological replicates. *$p < 0.05$ **$p < 0.001$ by Welch's *t* test. (D) Carboxysome foci intensity for specified cell strains. (arbitrary units = AU). WT $n = 1925$ foci; mNG-McdA[K15R] $n = 983$ foci; Δ*mcdB*, mNG-McdA[K15R] $n = 820$ foci. (E) Carboxysome foci number as a function of cell length. WT $n = 578$ cells; mNG-McdA[K15R] $n = 510$ cells; Δ*mcdB*, mNG-McdA[K15R] $n = 370$ cells. (F) Spacing of carboxysome foci. WT $n = 558$ cells; mNG-McdA[K15R] $n = 337$ cells; Δ*mcdB*, mNG-McdA[K15R] $n = 266$ cells. (G) Distribution of spacing between carboxysome foci as a function of cell length. WT $n = 558$ cells; mNG-McdA[K15R] $n = 530$ cells; Δ*mcdB*, mNG-McdA[K15R] $n = 380$ cells. (**H**) Microscopy images of mNG-McdA[K15R] (yellow), carboxysome foci (cyan), and DAPI-stained nucleoid (magenta) with ciprofloxacin

when they have no partition system at all (Youngren and Austin, 1997). Given the severity of the mutation, the mechanism for the Par^{PD} phenotype has not been directly identified in vivo. However, the inability to disassemble the DNA-ParA[K122R]-ParB-plasmid complex in vitro suggests a likely mechanism (Hwang *et al.*, 2013; Vecchiarelli *et al.*, 2013).

Strikingly, the corresponding mutation, mNG-McdA[K15R], resulted in nearly complete colocalization with carboxysomes (PCC = 0.83, $n = 558$ cells) (Figure 3A; Supplemental Table S2). When *mcdB* was deleted from this strain, mNG-McdA[K15R] no longer associated with carboxysomes (PCC = 0.60, $n = 391$ cells), instead, coating the nucleoid, thus showing its ability to still bind nsDNA (Figure 3B). The data suggest that the predicted ATP-trap mutant, McdA[K15R], locks carboxysomes onto the nucleoid via a more stable association with McdB. Consistently, bacterial two-hybrid (B2H) analysis also suggested that McdA[K15R] more stably associates with McdB compared with wild-type McdA (Figure 3C). However, immunoblot analysis showed that this increased signal may be due to McdA[K15R] being produced at higher levels than wild-type McdA. All other McdA mutants studied thus far showed no interaction with McdB via B2H analysis. But in this case, immunoblot analysis revealed that all McdA mutants predicted to be defective for dimerization (K15A, K15Q, G11V, and D39A) had significantly lower cellular levels compared with wild type and the K15R variant when expressed in *Escherichia coli*. Taken together, it is possible that the increased B2H signal for McdA[K15R] is due to this predicted ATP-trap mutant being a more stable dimer compared with wild-type McdA or the predicted dimerization-deficient mutants of McdA.

Compared to wild type, the McdA[K15R] mutant displayed significantly higher carboxysome foci intensities, a phenotype that was dependent on the presence of McdB (Figure 3D). Consistent with carboxysome aggregation, the McdA[K15R] mutant displayed fewer carboxysome foci per unit cell length (Figure 3E). The data suggest that McdB-stimulated ATP hydrolysis by McdA is required to disaggregate and distribute carboxysomes in the cell.

The predicted ATP-Trap mutant McdA[K15R] locks McdB-bound carboxysomes onto the nucleoid

Intriguingly, McdA[K15R] in the *mcdB* deletion strain displayed increased carboxysome spacing and variability in spacing, as cell length increased (Figure 3, F and G), a phenotype that is identical to an *mcdA* null mutant (Rillema *et al.*, 2021). With McdB present, however, the McdA[K15R] strain had carboxysome spacing closer to that of wild type (Figure 3F). Unique to the McdA[K15R] mutant, carboxysome foci were enriched within the midcell region (Supplemental Figure S3). Also, unlike all other McdA mutants described thus far, which were diffuse in the cytoplasm with nucleoid-excluded carboxysomes, mNG-McdA[K15R] strongly colocalized with carboxysomes (PCC = 0.91, $n = 303$ cells) over ciprofloxacin-compacted nucleoids (Figure 3H; Supplemental Table S2). In the Δ*mcdB* background, mNG-McdA[K15R] remained associated with the compacted nucleoid (PCC 0.90, $n = 346$), once again showing this mutant retains nonspecific DNA-binding activity, while carboxysomes became nucleoid excluded (PCC = 0.37, $n = 346$) (Figure 3I). Together, the data show that the predicted ATP-trap mutant McdA[K15R] locks carboxysome aggregates onto the nucleoid via a more stable association with McdB.

Finally, we asked if locking carboxysome aggregates onto the nucleoid in the McdA[K15R] strain resulted in the same cell elongation phenotype found for all other McdA mutants described thus far. Surprisingly, the McdA[K15R] strain did not elongate (Figure 3J). In fact, the McdA[K15R] cells were slightly smaller than wild type. We performed multigenerational time-lapse microscopy (Supplemental Movie S3) and found that McdA[K15R] cells are smaller than wild type because the mutant cells have a reduced growth rate (Figure 3K) as well as a longer doubling time (Figure 3L). When *mcdB* was deleted in the McdA[K15R] strain, the cell elongation phenotype returned (Figure 3J). The findings suggest that the pseudopositioning of carboxysome aggregates locked onto the nucleoid is sufficient to prevent cell elongation induced by the mispositioning of nucleoid-excluded carboxysome aggregates. But, locking carboxysome aggregates onto the nucleoid still compromises cell growth.

McdA represents an unstudied subclass of ParA family ATPases

Despite the McdA structure adopting an ATP-sandwich dimer as shown for other ParA ATPases (Schumacher *et al.*, 2019), McdA lacks the classical "signature lysine" residue in the deviant Walker A box that defines this family (see Figure 1B). Instead, the McdA structure identified a lysine residue, not only outside of the deviant Walker A box but in the C-terminal half of the protein at position 151, which is employed as the signature lysine (Figure 4A) (Schumacher *et al.*, 2019). As with the classical signature lysine, Lys151 interacts with the ATP molecule bound in the adjacent McdA monomer, making the same cross-contacts to the oxygen atom connecting the β- and γ-phosphates. Sequence alignments of McdA homologues that lack the classical signature lysine in the deviant Walker A box invariably encode for a lysine that corresponds to Lys151 in *S. elongatus* McdA (Figure 4A). Given the McdA structure, sequence conservation, and biochemical data suggesting Lys151 is important for ATP binding and dimerization (Schumacher *et al.*, 2019), we next observed the effect of mutating Lys151 to an alanine in vivo. The majority of mNG-McdA[K151A] remained diffuse in the cytoplasm, while a minor fraction colocalized with few and irregularly spaced carboxysome aggregates (PCC = 0.76, $n = 365$ cells) (Figure 4B; Supplemental Table S2). Carboxysome foci intensity, spacing, and average cell length were identical to those found for the other predicted ATP-binding and dimerization mutants of McdA tested in this study (Supplemental Figure S4, A–D). Also, ciprofloxacin treatment showed carboxysome aggregates were nucleoid excluded (PCC = 0.55, $n = 301$ cells) and once again butted up against the nucleoid poles (Figure 4C). The findings highlight the importance of Lys151

treatment. Merged image shows mNG-McdA[K15R] and carboxysome signals and the PCC value calculated from these two signals. (I) Microscopy images of mNG-McdA[K15R] (yellow), carboxysome foci (cyan), and DAPI-stained nucleoid (magenta) in the Δ*mcdB* background strain treated with ciprofloxacin. Merged image overlays all three channels. PCC value (top) is for colocalization between mNG-McdA[K15R] and DAPI signals. *PCC value (bottom) is for colocalization between DAPI and carboxysome signals. All PCC values were calculated from at least 300 cells per population. (J) Cell lengths of specified strains. WT $n = 558$ cells; mNG-McdA[K15R] $n = 337$ cells; Δ*mcdB*, mNG-McdA[K15R] $n = 266$ cells. Scale bars: 5 μm. (K) Growth rate of mNG-McdA and mNG-McdA[K15R] strains. For both strains $n = 300$ cells. (L) Doubling time of mNG-McdA and mNG-McdA[K15R] strains. WT $n = 222$ cells; mNG-McdA[K15R] $n = 296$ cells. Data represent median with interquartile range. ****$p < 0.0001$ by Welch's *t* test.

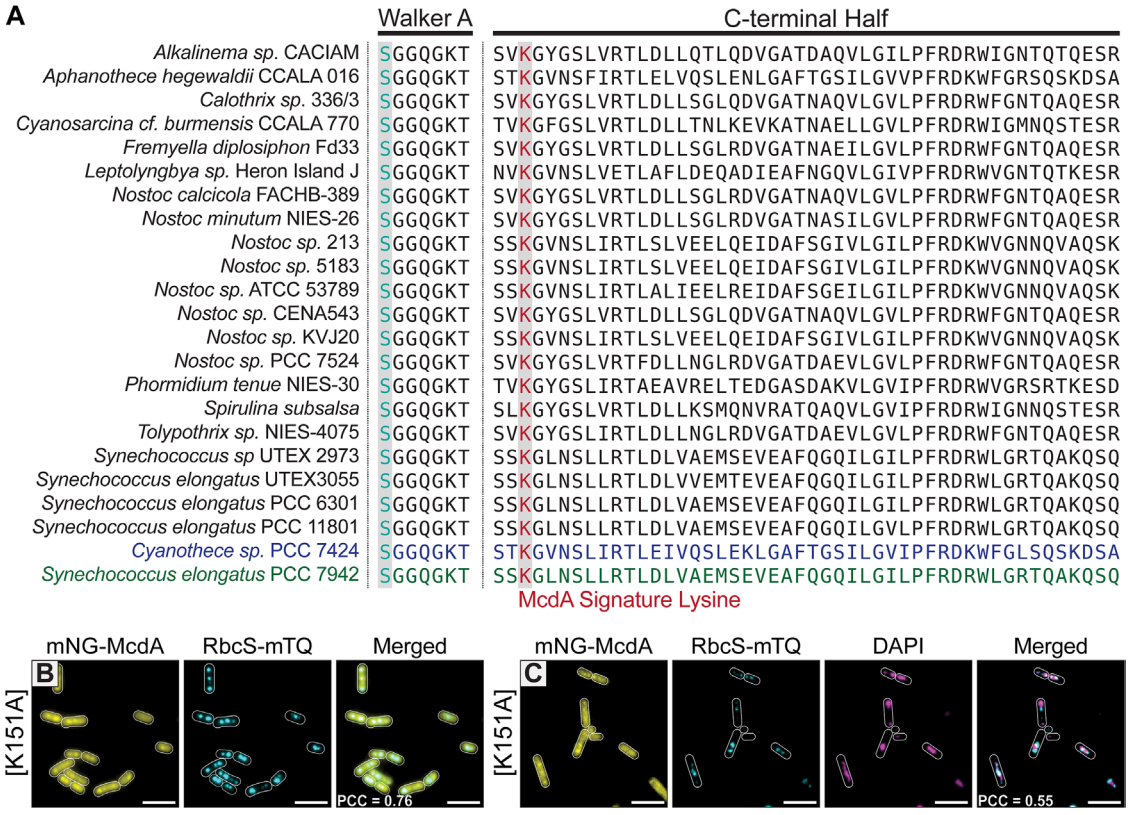

FIGURE 4: McdA is a member of an unstudied subclass of ParA-type ATPase characterized by a different signature lysine position. (A) Sequence alignment of McdA homologues possessing a serine residue in place of the signature lysine the Walker A box that co-occurs with an invariant lysine residue in the C-terminal half of protein—the McdA signature lysine. (B) Microscopy images of mNG-McdA[K151A] and RbcS-mTQ-labeled carboxysomes (cyan). Merged image shows mNG-McdA[K151A] and carboxysome signals and the PCC value calculated from these two signals. (C) Microscopy images of mNG-McdA[K151A] (yellow), carboxysome foci (cyan), and DAPI-stained nucleoid (magenta) with ciprofloxacin treatment. Merged image shows carboxysome and DAPI signals and the PCC value calculated from these two signals. PCC values were calculated from at least 300 cells per cell population. Scale bars: 5 μm.

as the "signature lysine" for an unstudied ParA subclass in forming the ATP-bound McdA dimer competent for nucleoid binding and positioning carboxysomes.

Moving the signature lysine of McdA into the Walker A box reconstitutes carboxysome pseudopositioning

Remarkably, Lys151 of the McdA structure overlays exceptionally well onto the signature lysine position in the deviant Walker A box of classical ParA family members (Schumacher *et al.*, 2019). This finding suggested that it may be possible to maintain carboxysome positioning with an McdA mutant that has its signature lysine at position 151 reintroduced into the classical position in the deviant Walker A box at position 10 (see Figure 4A). To make the signature lysine mutant, McdA[S10K, K151S], we swapped the serine at position 10 in the deviant Walker A box with the lysine at position 151. The mNG-McdA[K151S] phenotype mirrored that of McdA[K151A]—largely diffuse in the cytoplasm with nucleoid-excluded carboxysome aggregates (PCC = 0.53, n = 325 cells) (Supplemental Figure S4E; Supplemental Table S2). Immunoblot analysis verified that the diffuse localization of mNG-McdA[K151S] was not due to cleavage of the fusion protein (Supplemental Figure S1A). The mNG-McdA[S10K, K151S], on the other hand, largely colocalized with carboxysome foci (PCC = 0.84, n = 320 cells) (Figure 5A; Supplemental Table S2). Also, carboxysome spacing (Figure 5B) and intensity (Figure 5C) both trended back toward wild-type values, and ciprofloxacin treatment showed that carboxysomes strongly colocalized with mNG-McdA[S10K, K151S] (PCC = 0.85, n = 309 cells) and were now positioned within the nucleoid region of the cell (PCC = 0.78, n = 309 cells) (Figure 5D). Together, the data suggest a pseudorestoration of carboxysome positioning on the nucleoid. Consistently, the McdA[S10K, K151S] cell population had cell lengths revert back to wild type (Figure 5E), suggesting this pseudopositioning of carboxysomes is sufficient to alleviate the cell elongation mutant phenotype.

DISCUSSION

Members of the ParA family of ATPases position a wide variety of genetic and proteinaceous cargos involved in diverse biological processes (Lutkenhaus, 2012; Vecchiarelli *et al.*, 2012; Kiekebusch and Thanbichler, 2014). ATP cycling by the ParA ATPase is critical for its dynamic patterning behavior in the cell as well as its positioning activity on the cognate cargo. We recently found that the McdAB system is widespread across cyanobacteria and carboxysome-containing proteobacteria (MacCready *et al.* 2020; MacCready and Tran *et al.* 2021), yet it remains unknown how the ATPase cycle of McdA controls its oscillatory dynamics and its function in distributing carboxysomes across the nucleoid length. Several well-researched amino acid substitutions in the conserved ATP-binding site of ParA family ATPases have been used to trap the ATP cycle at specific

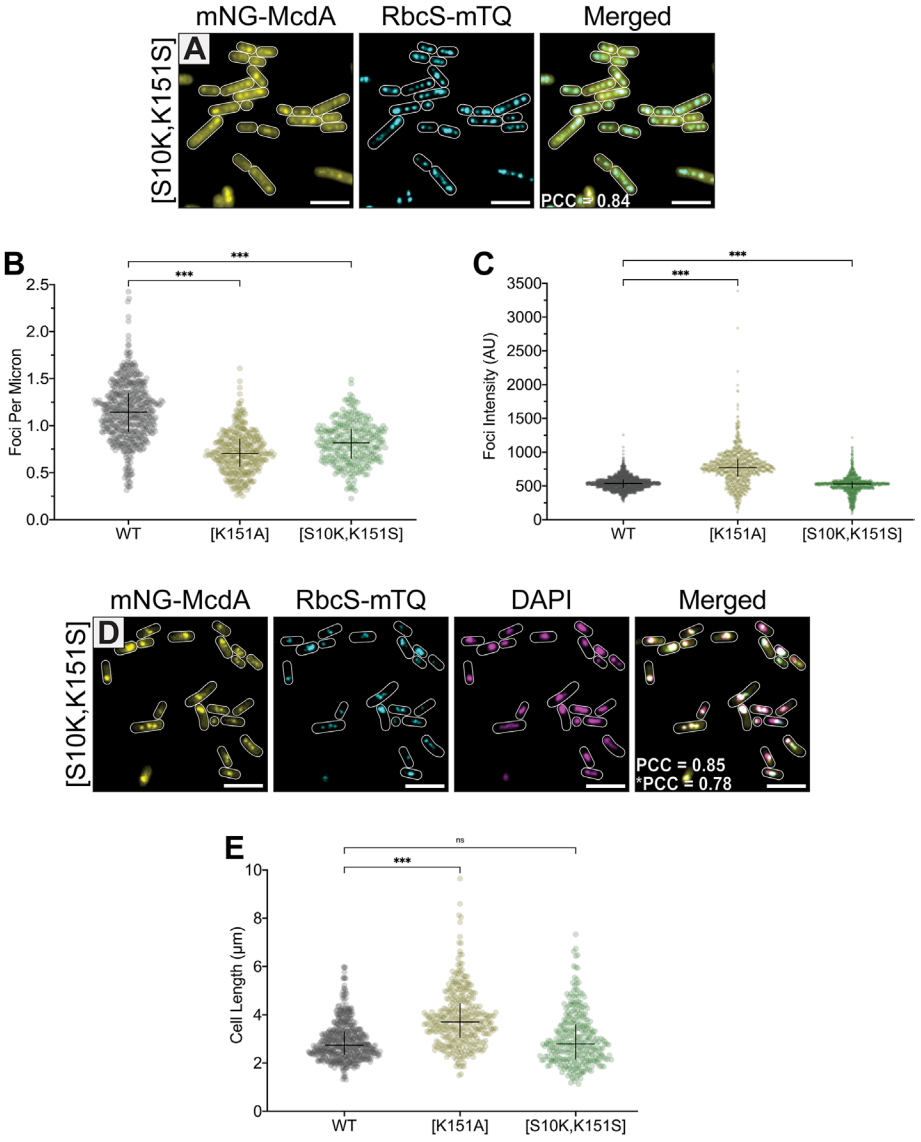

FIGURE 5: Carboxysomes are pseudopositioned when the McdA signature lysine is moved into the classical Walker A box position. (A) Microscopy images of mNG-McdA[S10K, K151S] and RbcS-mTQ-labeled carboxysomes (cyan). Merged image shows the overlay and calculated PCC values of these two signals. (B) Number of carboxysome foci per unit cell length. WT $n = 578$ cells; mNG-McdA[K151A] $n = 369$ cells; mNG-McdA[S10K,K151S] $n = 320$ cells. (C) Carboxysome foci intensity. (arbitrary units = AU). WT $n = 1925$ foci; mNG-McdA[K151A] $n = 965$ foci; mNG-McdA[S10K,K151S] $n = 1055$ foci. (D) Microscopy images of mNG-McdA[S10K, K151S] (yellow), carboxysome foci (cyan), and DAPI-stained nucleoid (magenta) with ciprofloxacin treatment. Merged image overlays carboxysome, mNG-McdA[S10K, K151S] and DAPI signals. PCC value (top) is for colocalization between mNG-McdA[S10K, K151S] and carboxysome signals. *PCC value (bottom) is for colocalization between DAPI and carboxysome signals. All PCC values were calculated from at least 300 cells per population. (E) Cell lengths of specified strains. ***$p < 0.001$, ns = not significant by Kruskal–Wallis test. WT $n = 561$ cells; mNG-McdA[K151A] $n = 365$ cells; mNG-McdA[S10K,K151S] $n = 320$ cells. Scale bars: 5 µm.

steps. These trap mutants have served as useful probes for dissecting the molecular steps involved in ParA-based positioning reactions (summary in Figure 1C, detailed in Supplemental Table S1). To dissect how ATP mediates McdA function in positioning fluorescently labeled carboxysomes, we introduced synonymous amino acid substitutions in the ATP-binding pocket of fluorescently labeled McdA to trap it at specific steps of the ATP cycle. While we are currently unable to purify and biochemically characterize the McdA variants used in this study, the phenotypes of these trap mutants have allowed us to correlate the known biochemistry of well-studied ParA family ATPases with specific steps in McdA action we observed here in vivo.

Overall, our findings suggest that ATP binding, dimerization, and an ATP-specific conformational change in McdA are all prerequisite steps for McdA to associate with the nucleoid via nonspecific DNA-binding activity (Figure 6A). Our findings also suggest that McdB-bound carboxysomes can only interact with McdA in this DNA-binding state. Nucleoid-associated McdA tethers McdB-bound carboxysomes to the nucleoid. But ultimately, McdB stimulates ATP hydrolysis by McdA, which reverts McdA back into its monomeric form that can no longer bind the nucleoid in the vicinity of the carboxysome. Through this Brownian-ratchet mechanism (MacCready *et al.*, 2018), McdB-bound carboxysomes are uniformly distributed as they locally generate McdA depletion zones on the nucleoid and then move up the resulting McdA gradient toward higher concentrations (Figure 6B).

McdA mutants predicted to be unable to bind ATP, dimerize, or undergo the ATP-specific conformational change required for nucleoid binding were diffuse in the cytoplasm, and carboxysomes were observed as nucleoid-excluded aggregates. These mutant strains also displayed cell elongation. We have recently shown that *mcdA* and *mcdB* deletion strains also elongate (Rillema *et al.*, 2021). Heterotrophic bacteria have been shown to undergo cell elongation as a carbon-limitation response (Rangarajan *et al.*, 2020). We also recently proposed that carboxysome aggregation results in decreased carbon-fixation efficiency, and that cell elongation is a response triggered by the resulting carbon limitation in this photoautotroph (Rillema *et al.*, 2021). Since the phenotype of these predicted McdA trap mutants mirrors the *mcdA* deletion strain, our findings suggest a complete loss of function in carboxysome positioning when McdA cannot bind ATP, dimerize, and adopt its nucleoid-binding conformation.

Nucleoid-excluded carboxysomes are trapped at the cytoplasm–nucleoid interface

We previously showed that in Δ*mcdA* or Δ*mcdB* strains of *S. elongatus*, carboxysomes still fully assemble, but coalesce into nucleoid-excluded aggregates (MacCready *et al.*, 2018). Given the polyploid nature of *S. elongatus*, there is insufficient cytoplasmic space to resolve whether carboxysomes aggregated due to physical interactions with each other or if they simply coalesced because of

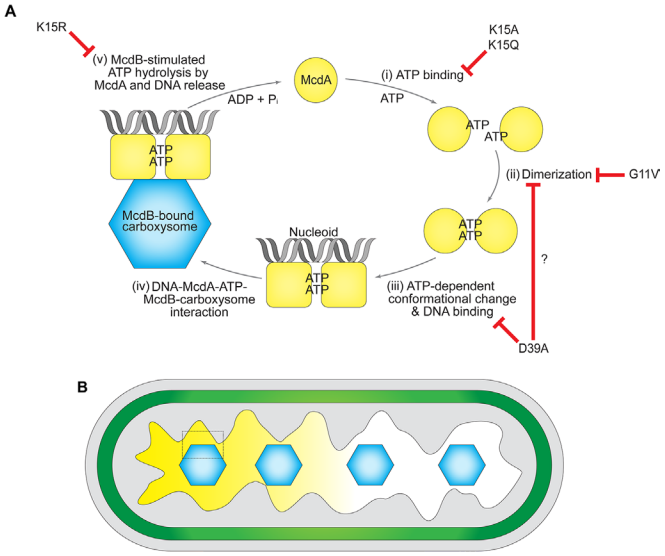

FIGURE 6: Model for ATP-cycling by McdA and associated functions in carboxysome positioning. (A) The ATPase cycle of McdA. Trap mutants of McdA predicted in this study are indicated. (i) When unbound from ATP, McdA monomers are diffuse in the cytoplasm. (ii) On ATP binding, McdA is competent for dimerization. (iii) ATP-bound McdA dimers must go through an ATP-dependent conformational change that licenses nsDNA binding to the nucleoid. (iv) McdB-bound carboxysomes are tethered via interactions with McdA-ATP dimers on the nucleoid. (v) McdB stimulates McdA ATPase activity and its release from the nucleoid in the vicinity of a carboxysome. (B) McdB-bound carboxysomes are uniformly distributed as they continually move toward higher concentrations of McdA on the nucleoid. The dashed box indicates the cellular region where step (iv) occurs in A.

nucleoid exclusion. We used the gyrase-inhibitor ciprofloxacin to compact the nucleoid and increase the cytoplasmic space of *S. elongatus* cells. Surprisingly, we found that in the absence of a functional McdAB system, carboxysome aggregates did not diffuse into the increased cytoplasmic space of ciprofloxacin-treated cells. Instead, the aggregates were maintained at the cytoplasm–nucleoid interface. It was recently shown that large plasmids lacking their ParA-based partition system, or large DNA circles excised from the chromosome, also localize to this interface (Planchenault *et al.*, 2020). This phenomenon was plasmid-size dependent; only plasmids larger than 100 kb preferentially localized to the nucleoid edge and did not diffuse into the nucleoid-free cytoplasmic space of the cell. Our findings here show that this preferential localization to the nucleoid edge is not specific to plasmids but rather is a widespread phenomenon in bacteria for both genetic and proteinaceous complexes on the mesoscale. Given the size dependence of nucleoid-evicted complexes being unable to penetrate the cytoplasm, we believe the most parsimonious explanation is that carboxysomes, and other mesoscale complexes, perceive the cytoplasmic environment as glassy (Parry *et al.*, 2014) and thus exhibit caging and subdiffusive behaviors at the nucleoid–cytoplasm interface.

Remarkably, wild-type cells treated with ciprofloxacin still displayed mNG-McdA oscillations and carboxysomes were still distributed over the highly compacted nucleoid (Supplemental Movie S2). The data suggest that the McdAB system can distribute carboxysomes regardless of whether the nucleoid is expanded or in an extremely compacted state. This finding has implications for identifying the forces responsible for carboxysome movement and positioning within the nucleoid region of the cell.

The predicted ATP-trap mutant McdA[K15R] locks carboxysomes onto the nucleoid

We identified the predicted ATP-trap mutant, McdA[K15R], that locks the nucleoid-McdA-McdB-carboxysome ternary complex. In the absence of McdB, mNG-McdA[K15R] still coated the nucleoid showing that it retains nonspecific DNA-binding activity, but carboxysomes were nucleoid excluded. In the presence of McdB, mNG-McdA[K15R] completely colocalized with massive carboxysome aggregates over the nucleoid. Together the findings show that McdA on the nucleoid transiently interacts with McdB on carboxysomes. McdB then stimulates McdA ATP hydrolysis and release from the nucleoid in the vicinity of carboxysomes, which allows for continued movement up the resulting McdA gradient. When McdB cannot stimulate the ATPase activity of McdA[K15R], the stable association tethers carboxysomes to the nucleoid. Since the ATP cycle cannot rest, McdB-bound carboxysomes act as a sink for all McdA[K15R] in the cell, which explains the lack of mNG-McdA[K15R] redistribution across the nucleoid.

All McdA mutants that resulted in nucleoid-excluded carboxysome aggregation also showed a cell elongation phenotype. The McdA[K15R] strain, on the other hand, displayed carboxysome aggregates on the nucleoid and no cell elongation phenotype. In contrast, the cells were slightly shorter than wild type due to reduced growth rate. We have two hypotheses that could explain this phenotype. First, tethering carboxysomes to the nucleoid could allow for pseudopositioning of carboxysomes. This "pilot-fish" mode of carboxysome positioning and inheritance could sufficiently improve carbon-fixation efficiency, thereby preventing carbon limitation and the cell elongation response. Even though elongation was prevented, tethering carboxysomes to the nucleoid still resulted in smaller cells and a slower growth rate. It is plausible that carboxysomes locked on the nucleoid have detrimental effects to a variety of DNA transactions such as DNA replication, transcription, nucleoid organization and compaction, and faithful chromosome segregation.

Swapping the signature lysine position in McdA resulted in carboxysome pseudopositioning on the nucleoid

McdA represents a previously unstudied subclass of the ParA family, where the signature lysine residue that defines this ATPase family is located in the C-terminal half of the protein, rather than in the Walker A box (see Figure 4A). We find here that lysine151 is indeed necessary for McdA to bind the nucleoid and position carboxysomes. Strikingly, we also found that repositioning this lysine into the classical signature lysine position in the Walker A box reconstituted carboxysome pseudopositioning—carboxysome spacing and focal intensity trended back to wild-type values. This mutant also reverted back to wild-type cell lengths. However, the oscillatory dynamics observed with wild-type McdA were not reconstituted. Instead, mNG-McdA[S10K, K151S] colocalized with carboxysomes over the nucleoid. This mode of carboxysome positioning is similar to that observed for the P1 plasmid partition system. P1 ParB forms punctate foci by loading onto and around a DNA-binding site called *parS* on the plasmid to be partitioned (Erdmann *et al.*, 1999; Sengupta *et al.*, 2010). The ParA ATPase uniformly distributes over the nucleoid but also forms foci that colocalize with relatively immobile ParB-bound plasmids (Hatano and Niki, 2010). During plasmid partitioning and movement, the colocalized ParA foci disappear and only reappear once the sister plasmids have reached the ¼ and

¾ positions of the cell where they once again become relatively immobile. McdA has an ATPase activity two orders of magnitude greater than ParA ATPases with a classical signature lysine (MacCready *et al.*, 2018). It is attractive to speculate that the lysine-swap mutant of McdA decreases its voracious ATPase activity, causing it to remain associated with McdB-bound carboxysomes for a longer period and adopting a "stick-and-move" mode of carboxysomes positioning over the nucleoid, similar to the P1 plasmid partition reaction described above. While we are currently unable to purify these McdA variants, a future direction will be to determine their ATPase activities compared with wild-type McdA to directly test this proposal.

Why does McdA have such a greater ATPase rate compared with classical ParA-type ATPases? We believe the answer lies in the difference in cargo copy-number in the cell. ParA-based DNA segregation systems are typically found on bacterial chromosomes and large low-copy plasmids. In both cases, the DNA is replicated and the sister copies are then segregated to opposing halves of the cell prior to division. Carboxysome copy number, on the other hand, can be significantly higher and varies depending on growth conditions. For example, when grown with high-light intensity, a single *S. elongatus* cell can contain up to a dozen carboxysomes (Sun *et al.*, 2016). We propose that for high-copy-number cargos, an increased ATPase activity is required to compensate for the decreased nearest-neighbor distance between adjacent cargos sharing the same nucleoid matrix. The increased ATPase rate would make the McdA gradient on the nucleoid more sensitive to carboxysome movements over these smaller spatial scales.

MATERIALS AND METHODS

Request a protocol through *Bio-protocol*.

Construct design

All constructs were made using Gibson assembly (Gibson *et al.*, 2009) from PCR fragments or synthesized dsDNA (Integrated DNA Technologies) and verified by Sanger sequencing (Supplemental Table S3). For *mcdB* deletion and native fluorescent fusion gene insertions into the *S. elongatus* genome, constructs were made as previously described (MacCready *et al.*, 2018). For fluorescent McdA mutants, the fluorescent protein mNG was inserted upstream of the mutated *mcdA* coding sequence with a GSGSGS linker. A 700-bp region upstream and downstream of the *mcdA* coding sequence was chosen as the homology regions required for replacing the native *mcdA* with mNG-tagged McdA mutants. A duplicate *mcdA* promoter and kanamycin resistance cassette were inserted upstream of the native *mcdA* promoter to prevent operon disruption. A second copy of the *rbcS* promoter and gene, tagged at the 3′ end with the fluorescent protein mTQ with a GSGSGS linker, was inserted at NS1 to serve as the carboxysome reporter gene. For *mcdB* deletion lines, a 700-bp region downstream of the *mcdB* coding region was chosen as the downstream homology region for insertion of fluorescent McdA mutants under its native promoter.

Growth conditions and transformations

All *S. elongatus* (ATCC 33912) strains were grown in 125-ml baffled flasks (Corning) in 50 ml BG-11 medium (Sigma), pH 8.3, buffered with 1 g/l HEPES. Cells were cultured in a Minitron incubation system (Infors-HT) with the following growth conditions: 60 µmol m^{-2} s^{-1} continuous LED 5600 K light, 32°C, 2% CO_2, and shaking at 130 RPM. Plasmids were cloned in chemically competent One Shot TOP10 *E. coli* cells (Thermo Fisher Scientific) in standard manipulation and culture conditions (Green and Sambrook 2012). Transformations of *S. elongatus* cells were performed as previously described (Clerico *et al.*, 2007). Transformant cells were plated on BG-11 agar with 12.5 µg/ml kanamycin, 12.5 µg/ml chloramphenicol, or 25 µg/ml spectinomycin. Single colonies were picked and transferred into 96-well plates containing BG-11 medium with corresponding antibiotic concentrations. Complete gene insertions and absence of the wild-type gene were verified via PCR, and cultures were removed from antibiotic selection by three series of back dilution prior to imaging.

Ciprofloxacin treatment and nucleoid visualization

To induce nucleoid compaction, *S. elongatus* cells were incubated with 50 µM ciprofloxacin overnight under normal growth conditions. To visualize the compacted nucleoid region, ciprofloxacin-treated *S. elongatus* cells were harvested by centrifugation at 13,000 × *g* for 1 min. The pelleted cells were then washed and resuspended in 100 µl of phosphate-buffered saline (pH 7.2). DAPI (8 µl from a 20 µg/ml stock concentration) was added to the cell suspension followed by 20-min incubation in the dark at 30°C. DAPI-stained cells were washed twice with 1 ml H_2O and then resuspended in 100 µl H_2O prior to visualization using the DAPI channel.

Fluorescence and time-lapse microscopy

Exponentially growing cells (2 ml of cells at OD_{750} ~ 0.7) were harvested and spun down at 4000 × *g* for 1 min and resuspended in 200 µl fresh BG-11, and 2 µl were then transferred to a 1.5% UltraPure agarose (Invitrogen) + BG-11 square pad on a 35-mm glass-bottom dish (MatTek Life Sciences). All fluorescence and phase-contrast imaging were performed using a Nikon Ti2-E motorized inverted microscope controlled by NIS Elements software with a SOLA 365 LED light source, a 100× objective lens (Oil CFI Plan Apochromat DM Lambda Series for Phase Contrast), and a Photometrics Prime 95B back-illuminated sCMOS camera or Hamamatsu Orca-Flash 4.0 LTS camera. mNG-McdA variants were imaged using a "YFP" filter set (C-FL YFP, Hard Coat, High Signal-to-Noise, Zero Shift, Excitation: 500/20 nm [490–510 nm], Emission: 535/30 nm [520–550 nm], Dichroic Mirror: 515 nm). RbcS-mTQ-labeled carboxysomes were imaged using a "CFP" filter set (C-FL CFP, Hard Coat, High Signal-to-Noise, Zero Shift, Excitation: 436/20 nm [426–446 nm], Emission: 480/40 nm [460-500 nm], Dichroic Mirror: 455 nm). DAPI fluorescence was imaged using a standard "DAPI" filter set (C-FL DAPI, Hard Coat, High Signal-to-Noise, Zero Shift, Excitation: 350/50 nm [325–375 nm], Emission: 460/50 nm [435–485 nm], Dichroic Mirror: 400 nm).

For multigenerational time-lapse microscopy of mNG-McdA and mNG-McdA[K15R] strains, 2 µl of exponentially growing cells were spotted on 1.5% UltraPure agarose + BG-11 round pads cast in a 35-mm glass-bottom dish already preincubated at 30°C in 5% CO_2 for at least 24 h. To sustain photosynthetic growth of *S. elongatus* cells on the microscope stage top, cells were constantly illuminated by the microscope's SOLA LED light source fitted with a 515-nm longpass filter. Temperature, humidity, and CO_2 concentrations were controlled with a Tokai Hit Incubation System. NIS Elements software with JOBS acquisition upgrade was used to synchronize control of shutter for growth light and image acquisition. Cells were acclimated to stage top growth conditions (32°C, 5% CO_2, 60 µmol m^{-2} s^{-1} light) for at least 30 min before image acquisition. Videos were taken at one frame per hour for a duration of 22 h.

Image analysis

Image analysis including cell segmentation, quantification of cell length, foci number, intensity, and spacing were performed using

Fiji plugin MicrobeJ 5.13I (Schindelin *et al.*, 2012; Ducret *et al.*, 2016). Cell perimeter detection and segmentation were done using the rod-shaped descriptor with default threshold settings. Carboxysome detection was performed using the smoothed foci function with tolerance of 50 and Z-score of 30. PCC values for merged signals were calculated using Fiji plugin JACoP (Just Another Colocalization Plugin) 2.1.1 (Bolte & Cordelières 2006). Data were exported, further tabulated, graphed, and analyzed using GraphPad Prism 9.0.1 for macOS (GraphPad Software, San Diego, CA, www.graphpad.com).

B2H and β-galactosidase activity assay

N-terminal T18 and T25 fusions of McdA, all McdA mutant variants, and McdB were constructed using the plasmids pKT25 and pUT18C. Plasmids were sequence-verified and cotransformed into *E. coli* BTH101 in both pairwise combinations (Karimova *et al.*, 1998). Several colonies of T18/T25 cotransformants were cultured in LB medium with 100 mg/ml ampicillin, 50 mg/ml kanamycin, and 0.5 mM IPTG overnight at 30 C with 225 rpm shaking. Overnight cultures were spotted on indicator LB X-gal plates supplemented with 100 mg/ml ampicillin, 50 mg/ml kanamycin, and 0.5 mM IPTG. Plates were incubated in the dark at 30°C up to 48 h before imaging. To quantify the interactions between hybrid proteins (Miller 1972), β-galactosidase activity measurements were performed as previously described (Battesti and Bouveret, 2012) with slight modifications. Two hundred microliters of the overnight cultures were transferred into glass tubes containing 800 µl of Z buffer (45 mM $Na_2HPO_4.12H_2O$, 45 mM $NaH_2PO_4.H2O$, 10 mM KCl, 1 mM $MgSO_4.7H_2O$, 38.5 mM β-mercaptoethanol). A drop of 0.01% SDS and two drops of chloroform were added, followed by 10 s of vigorous and thorough shaking to facilitate cell permeabilization. Once chloroform settled to the bottom (~15 s after mixing), 50 µl of the reaction mix were transferred into a 96-well flat-bottom microplate filled with 150 µl Z buffer already pre-equilibrated at 28°C in a SpectraMax iD3 microplate reader (Molecular Devices). To start the reaction, 40 µl 0.4% *o*-nitrophenyl-β-d-galactoside was added and measurements at OD_{420} were taken every 2 min for 1 h at 28°C using the microplate reader. Concurrently, 50 µl of the overnight cultures were added to a well plate containing 150 µl LB for OD_{600} measurement in the microplate reader. β-galactosidase enzymatic activities, in Miller Units (MU), were calculated using the formula $MU = A_{420}/(\text{incubation time in minutes} \times \text{culture volume in milliliters} \times OD_{600})$.

Total protein and immunoblot analyses

For total protein analysis in *E. coli*, a 0.2-ml aliquot was lysed using a Qsonica sonication system (20 cycles—30 s on, 10 s off at 30% power) and centrifuged at 10,000 × *g* for 1 min at 4 °C. The protein content in the supernatant was measured using a Bradford assay kit (catalogue number 5000006; Bio-Rad Laboratories). Immunoblot samples from *E. coli* cells were prepared by adding an equal volume of 4× Laemmli sample buffer to cultures prior to boiling for 20 min. For immunoblot analyses of *S. elongatus* strains, cultures were concentrated to an OD_{750} of 3 when harvesting. Immunoblot samples were generated by lysing cells with a Qsonica sonication system (20 cycles—30 s on, 10 s off at 30% power) in 0.5 ml RuBisCO extraction buffer (50 mM EPPS at pH 8.1, 1% PVPP, 526 1 mM EDTA, 10 mM dithiothreitol (DTT), 0.1% Triton, and Sigma protease inhibitor). An equal volume of 2× Laemmli sample buffer was added to cell lysates and boiled for 20 min. Samples (55 µl) were loaded on a 4–12% Bis-Tris NuPAGE gel with wedge wells (Invitrogen). Gels were transferred onto a minisize polyvinylidene difluoride membrane (Bio-Rad) using a Trans-Blot Turbo system (Bio-Rad). The membrane was immunoprobed using a mouse monoclonal antibody raised against amino acids 1–400 of *Bordetella pertussis* adenylate cyclase toxin origin (Santa Cruz Biotechnology), Cya A (1:1000), or a rabbit polyclonal antisera against McdA (1:1000) (New England Peptide). The membrane was then incubated with the goat anti-Mouse IgG Secondary Antibody IRDye 800 CW (LI-COR) or the HRP–conjugated anti-Rabbit IgG secondary antibody (Milipore Sigma). Membrane signals were developed with 508 Femto Maximum Sensitivity Substrate (Thermo Scientific) and visualized and quantified using LI-COR Image Studio. The McdA signal was normalized to a nonspecific band as indicated in Supplemental Figure S1A.

Expression and purification of *Ct*McdA and *Ct*McdA[D38A]

Both *Ct*McdA and *Ct*McdA[D38A] were expressed and purified in a similar manner. For protein production, the expression plasmids for these constructs (Schumacher *et al.*, 2019) were transformed into *E. coli* C41(DE3) cells (Lucigen). Transformants were grown at 37°C and 225 rpm until an OD_{600} of 0.4–0.6 was reached. The culture flasks were rapidly cooled down to 15°C on and protein expression was then induced with the addition of 1 mM IPTG. After overnight induction, the cells were pelleted, flash-frozen in liquid nitrogen and stored at –80°C. Harvested cells were resuspended in Buffer A (25 mM Tris-HCl, pH 7.5, 300 mM NaCl, 10% glycerol, 0.5 mM BME, 50 mg/ml lysozyme, 1.25 kU benzonase, 2 protease inhibitor cocktail tablets) and lysed using a probe sonicator with 15 s on, 15 s off pulsation for 8 min. The lysate was cleared by centrifugation at 12,000 × *g* at 4 °C for 40 min in a Fiberlite TM F15-8 × 50 cy Fixed Angle Rotor (Thermo Fisher Scientific). The resulting lysate was filtered through a 0.45-µm syringe filter and loaded onto a 5-ml HiTrap TALON Crude cassette (GE) and eluted with a 0- to 400-mM imidazole gradient. Peak fractions were pooled and concentrated using an Amicon Ultra Centrifugal Device (10 KD MWCO). The concentrated protein sample was passed through a HiPrep 26/10 Desalting Column (GE) equilibrated in Q-Buffer (25 mM Tris-HCl, pH 7.5, 150 mM NaCl, 10% glycerol, 1 mM EDTA, 1 mM DTT). The sample was then immediately loaded onto a HiTrap Q HP 5 ml cassette (GE) equilibrated in Q-Buffer. The protein was eluted with a 150-mM to 2-M NaCl gradient. Peak fractions were concentrated to no more than 70 mM and flash-frozen aliquots were kept at –80°C.

DNA-binding assay

EMSAs were performed in a final reaction volume of 10 µl in a buffer containing 50 mM HEPES (pH 7.6), 5 mM $MgCl_2$, and 100 mM KCl with 10 nM pUC19 plasmid (2.8 kb) as the supercoiled DNA substrate. At the concentrations indicated, His-*Ct*McdA and His-*Ct*McdA[D38A] were incubated for 30 min at 23°C with or without ATP (1 mM). Reactions were then mixed with 1 µl 80% glycerol, run on 1% agarose gel in 1× TAE at 110V for 45 min, and stained with ethidium bromide prior to imaging.

Protein structure visualization and prediction

Molecular graphics and analyses of protein structures were performed with UCSF Chimera, developed by the Resource for Biocomputing, Visualization and Informatics at the University of California, San Francisco, with support from National Institutes of Health P41-GM103311 (Pettersen *et al.*, 2004). Prediction of *Se*McdA structure was performed with Phyre2 (Kelley *et al.*, 2016).

ACKNOWLEDGMENTS

We thank Joshua MacCready, Kiyoshi Mizuuchi, Maria Schumacher, and David Savage for helpful discussions. The pET15b expression vectors used for *Ct*McdA and *Ct*McdA[D38A] were kind gifts from Maria Schumacher. This work is supported by the National Science Foundation to A.G.V. (Award No. 1817478 and CAREER Award No. 1941966), Rackham Graduate Research Grant to P.H., Rackham Professional Development Grant to P.H., American Society for Microbiology Research Capstone Fellowship to P.H., Margaret Dow Towsley Scholarship to P.H., and by a research initiation fund to A.G.V. provided by the MCDB department, University of Michigan.

REFERENCES

Adler J, Parmryd I (2010). Quantifying colocalization by correlation: the Pearson correlation coefficient is superior to the Mander's overlap coefficient. Cytometry 77, 733–42.

Ah-Seng Y, Lopez F, Pasta F, Lane D, Bouet J-Y (2009). Dual role of DNA in regulating ATP hydrolysis by the SopA partition protein. J Biol Chem 284, 30067–30075.

Badrinarayanan A, Le TBK, Laub MT (2015). Bacterial chromosome organization and segregation. Annu Rev Cell Dev Biol 31, 171–199.

Barillà D, Rosenberg MF, Nobbmann U, Hayes F (2005). Bacterial DNA segregation dynamics mediated by the polymerizing protein ParF. EMBO J 24, 1453–1464.

Battesti A, Bouveret E (2012). The bacterial two-hybrid system based on adenylate cyclase reconstitution in Escherichia coli. Methods 58, 325–334.

Baxter JC, Funnell BE (2014). Plasmid partition mechanisms. Microbiol Spectr 2, PLAS-0023-2014.

Brannudd I, Karlsson E, Nordblom G, Sjogren M, Naslund LS, Stevrell J (2020). Unravelling the Mechanisms of Multifunctional Antibiotic Drugs. Thesis. Dept of Biology and Biological engineering, Chalmers University of Technology.

Bolte S, Cordelières FP (2006). A guided tour into subcellular colocalization analysis in light microscopy. J Microsc 224, 213–232.

Castaing JP, Bouet JY, Lane D (2008). F plasmid partition depends on interaction of SopA with non-specific DNA. Mol Microbiol 70, 1000–1011.

Clerico EM, Ditty JL, Golden SS (2007). Specialized techniques for site-directed mutagenesis in cyanobacteria. In: Circadian Rhythms: Methods and Protocols. ed. E. Rosato, New Jersey: Humana Press, 155–171.

Cohen Y, Gurevitz M (2006). The Cyanobacteria - Ecology, physiology and molecular genetics. In: The Prokaryotes: Volume 4: Bacteria: Firmicutes, Cyanobacteria. ed. M. Dworkin, S. Falkow, E. Rosenberg, K-H. Schleifer, E. Stackebrandted. New York: Springer, 1074–1098.

Corrales-Guerrero L, He B, Refes Y, Panis G, Bange G, Viollier PH, Steinchen W, Thanbichler M (2020). Molecular architecture of the DNA-binding sites of the P-loop ATPases MipZ and ParA from *Caulobacter crescentus*. Nucleic Acids Res 48, 4769–4779.

Davey M, Funnell BE (1997). Modulation of the P1 plasmid partition protein ParA by ATP, ADP, and P1 ParB. J Biol Chem 272, 15286–15292.

Ducret A, Quardokus EM, Brun YV (2016). MicrobeJ, a tool for high throughput bacterial cell detection and quantitative analysis. Nat Microbiol 1, 1–7.

Dunham TD, Xu W, Funnell BE, Schumacher MA (2009). Structural basis for ADP-mediated transcriptional regulation by P1 and P7 ParA. EMBO J 28, 1792–1802.

Erdmann N, Petroff T, Funnell BE (1999). Intracellular localization of P1 ParB protein depends on ParA and parS. Proc Natl Acad Sci USA 96, 14905–14910.

Fung E, Bouet J-Y, Funnell BE (2001). Probing the ATP-binding site of P1 ParA: partition and repression have different requirements for ATP binding and hydrolysis. EMBO J 20, 4901–4911.

Funnell BE (2016). ParB Partition Proteins: Complex formation and spreading at bacterial and plasmid centromeres. Front Mol Biosci 3, 44.

Gibson DG, Young L, Chuang RY, Venter JC, Hutchison CA, Smith HO (2009). Enzymatic assembly of DNA molecules up to several hundred kilobases. Nat Methods 6, 343–345.

Green MR, Sambrook J (2012). Molecular Cloning: A Laboratory Manual, Fourth Edition. New York: Cold Spring Harbor Laboratory Press.

Hatano T, Niki H (2010). Partitioning of P1 ParA plasmids by gradual distribution of the ATPase ParA. Mol Microbiol 78, 1182–1198.

Hatano T, Yamaichi Y, Niki H (2007). Oscillating focus of SopA associated with filamentous structure guides partitioning of F plasmid. Mol Microbiol 64, 1198–1213.

Hester CM, Lutkenhaus J (2007). Soj (ParA) DNA binding is mediated by conserved arginines and is essential for plasmid segregation. Proc Natl Acad Sci USA 104, 20326–20331.

Hwang LC, Vecchiarelli AG, Han YW, Mizuuchi M, Harada Y, Funnell BE, Mizuuchi K (2013). ParA-mediated plasmid partition driven by protein pattern self-organization. EMBO J 32, 1238–1249.

Jalal ASB, Le TBK (2020). Bacterial chromosome segregation by the ParABS system. Open Biol 10, 200097.

Karimova G, Pidoux J, Ullmann A, Ladant D (1998). A bacterial two-hybrid system based on a reconstituted signal transduction pathway. Proc. Natl. Acad. Sci. USA 95, 5752–5756.

Kelley LA, Mezulis S, Yates CM, Wass MN, Sternberg MJ (2016). The Phyre2 web portal for protein modeling, prediction and analysis. Nat Protoc 10, 845–858.

Kerfeld CA, Aussignargues C, Zarzycki J, Cai F, Sutter M (2018). Bacterial microcompartments. Nat Rev Microbiol 16, 277–290.

Kiekebusch D, Michie KA, Essen LO, Löwe J, Thanbichler M (2012). Localized dimerization and nucleoid binding drive gradient formation by the bacterial cell division inhibitor MipZ. Mol Cell 46, 245–259.

Kiekebusch D, Thanbichler M (2014). Spatiotemporal organization of microbial cells by protein concentration gradients. Trends Microbiol 22, 65–73.

Koonin EV (1993). A superfamily of ATPases with diverse functions containing either classical or deviant ATP-binding motif. J Mol Biol 229, 1165–1174.

Leonard TA, Butler PJ, Lowe J (2005). Bacterial chromosome segregation: structure and DNA binding of the Soj dimer - a conserved biological switch. EMBO J 24, 270–282.

Libante V, Thion L, Lane D (2001). Role of the ATP-binding site of SopA protein in partition of the F plasmid. J Mol Biol 314, 387–399.

Lin L, Osorio Valeriano M, Harms A, Søgaard-Andersen L, Thanbichler M (2017). Bactofilin-mediated organization of the ParABS chromosome segregation system in *Myxococcus xanthus*. Nat Commun 8, 1817.

Lutkenhaus J (2012). The ParA/MinD family puts things in their place. Trends Microbiol 20, 411–418.

Lutkenhaus J, Sundaramoorthy M (2003). MinD and role of the deviant Walker A motif, dimerization and membrane binding in oscillation. Mol Microbiol 48, 295–303.

MacCready JS, Basalla JL, Vecchiarelli AG (2020). Origin and evolution of carboxysome positioning systems in cyanobacteria. Mol Biol Evol 37, 1434–1451.

MacCready JS, Hakim P, Young EJ, Hu L, Liu J, Osteryoung KW, Vecchiarelli AG, Ducat DC (2018). Protein gradients on the nucleoid position the carbon-fixing organelles of cyanobacteria. eLife 7, e39723.

MacCready JS, Tran L, Basalla JL, Hakim P, Vecchiarelli AG (2021). The McdAB system positions α-carboxysomes in proteobacteria. Mol Microbiol 00, 1–21.

Ono H, Takashima A, Hirata H, Homma M, Kojima S (2015). The MinD homolog FlhG regulates the synthesis of the single polar flagellum of *Vibrio alginolyticus*. Mol Microbiol 98, 130–141.

Park KT, Wu W, Lovell S, Lutkenhaus J (2012). Mechanism of the asymmetric activation of the MinD ATPase by MinE. Mol Microbiol 85, 271–281.

Parry BR, Surovtsev IV, Cabeen MT, O'Hern CS, Dufresne ER, Jacobs-Wagner C (2014). The bacterial cytoplasm has glass-like properties and is fluidized by metabolic activity. Cell 156, 183–194.

Pettersen EF, Goddard TD, Huang CC, Couch GS, Greenblatt DM, Meng EC, Ferrin TE (2004). UCSF Chimera—A visualization system for exploratory research and analysis. J Comput Chem 25, 1605–1612.

Planchenault C, Pons CM, Shiavon C, Siguier P, Rech J, Guynet C, Dauverd-Girault J, Cury J, Rocha EPC, Junier I, *et al*. (2020). Intracellular positioning systems limit the entropic eviction of secondary replicons toward the nucleoid edges in bacterial cells. J Mol Biol 432, 745–761.

Pratto F, Cicek A, Weihofen WA, Lurz R, Saenger W, Alonso JC (2008). *Streptococcus pyogenes* pSM19035 requires dynamic assembly of ATP-bound ParA and ParB on parS DNA during plasmid segregation. Nucl Acids Res 36, 3676–3689.

Ptacin JL, Gahlmann A, Bowman GR, Perez AM, von Diezmann ARS, Eckart MR, Moerner WE, Shapiro L (2014). Bacterial scaffold directs centromere movement. Proc Natl Acad Sci USA 111, E2046–E2055.

Ptacin JL, Lee SF, Garner EC, Toro E, Eckart M, Comolli LR, Moerner WE, Shapiro L (2010). A spindle-like apparatus guides bacterial chromosome segregation. Nat Cell Biol 12, 791–798.

Rangarajan AA, Koropatkin NM, Biteen JS (2020). Nutrient-dependent morphological variability of *Bacteroides thetaiotaomicron*. Microbiology 166, 624–628.

Rillema R, Hoang Y, MacCready JS, Vecchiarelli AG (2021). Carboxysome mispositioning alters growth, morphology, and Rubisco level of the cyanobacterium *Synechococcus elongatus* PCC 7942. mBio 3, e0269620.
Ringgaard S, Zepeda-Rivera M, Wu X, Schirner K, Davis BM, Waldor MK (2014). ParP prevents dissociation of CheA from chemotactic signaling arrays and tethers them to a polar anchor. Proc Natl Acad Sci USA 111, E255–E264.
Ringgaard S, Van Zon J, Howard M, Gerdes K (2009). Movement and equipositioning of plasmids by ParA filament disassembly. Proc Natl Acad Sci USA 106, 19369–19374.
Roberts MAJ, Wadhams GH, Hadfield KA, Tickner S, Armitage JP (2012). ParA-like protein uses nonspecific chromosomal DNA binding to partition protein complexes. Proc Natl Acad Sci USA 109, 6698–6703.
Sanchez A, Cattoni DI, Walter J-C, Rech J, Parmeggiani A, Nollmann M, Bouet J-Y (2015). Stochastic self-assembly of ParB proteins builds the bacterial DNA segregation apparatus. Cell Syst 1, 163–173.
Savage DF, Afonso B, Chen AH, Silver PA (2010). Spatially ordered dynamics of the bacterial carbon fixation machinery. Science 327, 1258.
Schindelin J, Arganda-Carreras I, Frise E, Kaynig V, Longair M, Pietzsch T, Preibisch S, Rueden C, Saalfeld S, Schmid B, *et al*. (2012). Fiji: An open-source platform for biological-image analysis. Nat Methods 9, 676–682.
Schuhmacher JS, Rossman F, Dempwolff F, Knauer C, Altegoer F, Steinchen W, Dörrich AK, Klingl A, *et al*. (2015). MinD-like ATPase FlhG effects location and number of bacterial flagella during C-ring assembly. Proc Natl Acad Sci USA 112, 3092–3097.
Schumacher D, Bergeler S, Harms A, Vonck J, Huneke-Vogt S, Frey E, Søgaard-Andersen L (2017). The PomXYZ proteins self-organize on the bacterial nucleoid to stimulate cell division. Dev Cell 41, 299–314.
Schumacher MA, Henderson M, Zhang H (2019). Structures of maintenance of carboxysome distribution Walker-box McdA and McdB adaptor homologs. Nucleic Acids Res 47, 5950–5962.
Schumacher MA, Ye Q, Barge MT, Zampini M, Barillà D, Hayes F (2012). Structural mechanism of ATP-induced polymerization of the partition factor ParF: Implications for DNA segregation. J Biol Chem 287, 26146–26154.
Sengupta M, Nielsen HJ, Youngren B, Austin S (2010). P1 plasmid segregation: Accurate redistribution by dynamic plasmid pairing and separation. J Bacteriol 192, 1175–1183.
Shaner NC, Lambert GG, Chammas A, Ni Y, Cranfill PJ, Baird MA, Sell BR, Allen JR, Day RN, Israelsson M, *et al*. (2013). A bright monomeric green fluorescent protein derived from *Branchiostoma lanceolatum*. Nat Methods 10, 407–409
Sun Y, Casella S, Fang Y, Huang F, Faulkner M, Barrett S, Liu LN (2016). Light modulates the biosynthesis and organization of cyanobacterial carbon fixation machinery through photosynthetic electron flow. Plant Physiol 171, 530–541.
Thanbichler M, Shapiro L (2006). MipZ, a spatial regulator coordinating chromosome segregation with cell division in *Caulobacter*. Cell 126, 147–162.
Toro E, Hong S, McAdams HH, Shapiro L (2008). *Caulobacter* requires a dedicated mechanism to initiate chromosome segregation. Proc Natl Acad Sci USA 105, 15435–15440.
Treuner-Lange A, Aguiluz K, van der Does C, Gómez-Santos N, Harms A, Schumacher D, Lenz P, Hoppert M, Kahnt J, Muñoz-Dorado J, Søgaard-Andersen L (2013). PomZ, a ParA-like protein, regulates Z-ring formation and cell division in *Myxococcus xanthus*. Mol Microbiol 87, 235–253.
Turmo A, Gonzalez-Esquer CR, Kerfeld CA (2017). Carboxysomes: metabolic modules for CO2 fixation. FEMS Microbiol Lett 364.
Vecchiarelli AG, Han Y-W, Tan X, Mizuuchi M, Ghirlando R, Biertümpfel C, Funnell BE, Mizuuchi K (2010). ATP control of dynamic P1 ParA-DNA interactions: a key role for the nucleoid in plasmid partition. Mol Microbiol 78, 78–91.
Vecchiarelli AG, Havey JC, Ing LL, Wong EOY, Waples WG, Funnell BE (2013). Dissection of the ATPase active site of P1 ParA reveals multiple active forms essential for plasmid partition. J Biol Chem 288, 17823–17831.
Vecchiarelli AG, Mizuuchi K, Funnell BE (2012). Surfing biological surfaces: Exploiting the nucleoid for partition and transport in bacteria. Mol Microbiol 86, 513–523.
Vecchiarelli AG, Neuman KC, Mizuuchi K (2014). A propagating ATPase gradient drives transport of surface-confined cellular cargo. Proc Natl Acad Sci USA 111, 4880–4885.
Volante A, Alonso JC (2015). Molecular anatomy of ParA-ParA and ParA-ParB interactions during plasmid partitioning. J Biol Chem 290, 18782–18795.
Youngren B, Austin S (1997). Altered ParA partition proteins of plasmid P1 act via the partition site to block plasmid propagation. Mol Microbiol 25, 1023–1030.
Zhang H, Schumacher MA (2017). Structures of partition protein para with nonspecific DNA and ParB effector reveal molecular insights into principles governing Walker-box DNA segregation. Genes Dev 31, 481–492.
Zhou H, Schulze R, Cox S, Saez C, Hu Z, Lutkenhaus J (2005). Analysis of MinD mutations reveals residues required for MinE stimulation of the MinD ATPase and residues required for MinC interaction. J Bacteriol 187, 629–638.